

SQUID AND RELATED EXPERIMENTS

Kaling Vikram Singh¹

Abstract

The study includes a thorough theoretical analysis of the fundamental characteristics of superconductors, Josephson Junctions, and DC-SQUIDs. The three most significant phenomenological characteristics of superconductors: zero resistance, perfect diamagnetism, and macroscopic phase coherence have been introduced. Next, the fundamental characteristics of Josephson junctions RT, IV, and shapiro characteristics as well as their sensitivity to microwave signals have been covered. Two Josephson Junctions on a superconducting loop running parallel to one another make up a DC SQUID. The basic mechanism of SQUIDs have been explained to establish their flux-voltage conversion . The transition temperature of YBCO powder was determined using LC circuits, and experiments were carried out to determine various SQUID probe properties

Keywords

Super conductivity—SQUID—Transition temperature—YBCO

¹National Institute of Science Education and Research, Roll 2011074

*Corresponding author: kalingvikram.singh@niser.ac.in

Contents

1	Introduction	1
1.1	BCS Theory	2
1.2	Ginzberg - Landau Theory	3
	London penetration depth • Spatial Variation of order parameter	
1.3	Josephson junctions and SQUID	5
1.4	Shapiro effect	6
1.5	Resistance vs Temperature characteristics	6
1.6	SQUID chip	6
	SQUID parameters	
2	Experimental setup	7
2.1	Cryogenics	7
2.2	SQUID chip	7
2.3	Electrical equipments	7
3	Experiment and Observations	7
3.1	Experiment and problems incurred	7
	IV characteristics • V - phi characteristics • Shapiro steps • SQUID as a DC voltmeter • Transition temperature of YBCO	
3.2	Analysis and calculations	11
	Critical current, resistance, modulation depth and others • Flux per quanta and inductance • Shapiro steps • Transition temperature of YBCO	
4	Results	12
5	Conclusion	12
6	References	12
7	Appendix	13
7.1	Klystron wave generator	13
7.2	Frequency meter	13
7.3	Seelab	13

Objectives

- To study the working of SQUID
- To study the superconductor properties
- To find the transition temperature of YBCO

1. Introduction

Kammerlingh Onnes and his group were first, in 1911, to report the existence of a superconductor, namely a superconducting state of mercury at 4.2 Kelvin after liquifying Helium gas. Since then, different materials were tested for existence of the superconducting states and this lead to the theory of superconductivity.

Superconductors are materials with exceptional properties. Below a temperature, critical temperatures (T_c), superconductors lose all its electrical resistivity and become diamagnetic. These materials also show Meissner effect, the phenomena of expulsion of a magnetic field from a superconductor during its transition to the superconducting state when it is cooled below the critical temperature.

Superconductors are classified based on the strength of Meissner effect and critical temperature (T_c) as TYPE-1(low temperature superconductor) and TYPE-2 (high temperature superconductor). TYPE 1 superconductors have a $T_c \leq 10K$. They show perfect Meissner effect along perfect diamagnetism and very low critical field. The transition from non superconducting to superconducting of TYPE 1 superconductors is abrupt and show single critical fields. TYPE 2 semiconductors, on the other hand, have $T_c \geq 10K$. They partly show Meissner effect along with imperfect diamagnetism and comparatively

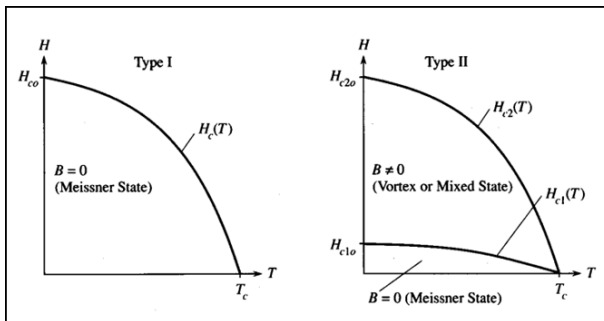


Figure 1. Type 1 and Type 2 superconductors [Hale].

higher critical fields. The transition of these superconductors has a mixed state that is between normal and the superconducting states, limited by two separate critical fields at the extremes of the mixed state as shown in 1.

In 1957, Bardeen-Cooper-Schrieffer (BCS) developed the theory of superconductivity to explain the physics behind superconductivity of TYPE 1 superconductors. The theory of superconductivity for TYPE 2 superconductors was given by Gilsberg and Landau in the same year.

1.1 BCS Theory

The BCS theory is based on the existence of Cooper pairs. Cooper pairs are a pair of electrons in a superconducting system which are attractively bounded to each other alongside having equal and opposite momenta and spins. Consider a pair of electrons just outside the fermi surface such that they have opposite momenta \vec{K} and $-\vec{K}$. The hamiltonian is given by:

$$H = 2 \sum_k \epsilon_k + \sum_k V_k \quad (1)$$

The states can be treated as superposition of multiple states, i.e., $\psi = \sum_k g_k \psi_k$. Using hamilton's equation, we have:

$$\begin{aligned} H\psi &= E\psi \\ g_k [E - 2 \sum_k \epsilon_k] &= \sum_{kk'} v_{kk'} g_{k'} \\ g_k &= \frac{\sum_{kk'} v_{kk'} g_{k'}}{E - 2 \sum_k \epsilon_k} \end{aligned} \quad (2)$$

Since g_k are amplitudes, $\sum_k g_k = 1$. The potential is given by:

$$V_{kk'} = \begin{cases} V & \text{if } E_0^f < E < h\omega_d + E_f^0 \\ 0 & \text{otherwise} \end{cases} \quad (3)$$

Thus, we get the integral:

$$\int_{E_0^f}^{E_0^f + h\omega_d} \frac{-VN(\epsilon)}{E - 2\epsilon} d\epsilon \quad (4)$$

Since the density of states is slowly varying function near the fermi surface, we can estimate it be $N(\epsilon) \sim N(E_0^f)$. Thus, the eq (4) integrates to:

$$\exp\left(\frac{2}{VN(E_0^f)}\right) = 1 - \frac{2\hbar\omega_d}{E - E_0^f} \quad (5)$$

This leads to a pairing energy gap Δ given by $\Delta = E - 2E_0^f$. For a weak coupling limit, Δ can be found through eq(5) as:

$$\Delta = 2\hbar\omega_d \exp\left(\frac{-2}{N(E_0^f)V}\right) \quad (6)$$

As long as the potential V is attractive and $N(E_0^f)V$ is finite, we see formation of bound pairs of electrons. These bound pair of electrons are called Cooper pairs. After pairing up, these Cooper pairs behave as bosons and loose their fermionic behaviors. Formation of Cooper pairs have two important consequences: (a) The attraction between electrons is phonon mediated, and (b) The coulomb potential is screened in the material due to presence of positive ions in the metal [Kita].

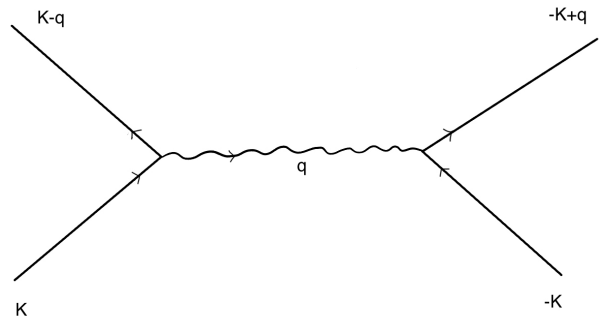


Figure 2. Electron - Phonon interaction.

For a metallic system with electron - phonon interaction (fig:2) > coulomb interaction, the formation of Cooper pairs is feasible. Classically, the displacement of the electrons from the mean position due to attractions towards positive ions lead to the electron - electron interaction mediated through a phonon. The pairing energy gap is experimentally verified and can be determined through methods like ultrasonic absorption below transition temperatures, IV characteristics of electron tunneling, etc. Other mechanisms such as plasma or magnons can also lead to cooper pair formation, but phonon mechanism is the most common mechanism observed. A system with strong electron-phonon interaction is a poor conductor of electricity at room temperature, but is a good superconductor at absolute zero temperatures. It is a common trait that good conductors of electricity are worse superconductors compared to poor conductors of electricity.

The BCS theory states that in a metallic system, all the electrons form cooper pairs. The corresponding energies and

eigen states can be found using the following way:

Let $\langle k| -k1 \rangle$ denote the cooper pair state. Let w_k denote the probability that a system has an occupied cooper pair state. Also, let $v_k^2 = w_k$. The general eigen state is given by:

$$|\psi_k\rangle = u_k |0\rangle_k + v_k |1\rangle_k \quad (7)$$

where, $|0\rangle_k$ is unoccupied state and $|1\rangle_k$ is the occupied cooper pair state and $|0\rangle_k = \begin{pmatrix} 0 \\ 1 \end{pmatrix}$ and $|1\rangle_k = \begin{pmatrix} 1 \\ 0 \end{pmatrix}$. Also define the annihilation and creation operators $\sigma^+ = (\sigma^1 + i\sigma^2)/2$ and $\sigma^- = (\sigma^1 - i\sigma^2)/2$, where σ^i are pauli matrices. Hence, we get the following relations:

$$\sigma^+ |0\rangle_k = |1\rangle_k, \sigma^+ |1\rangle_k = 0$$

$$\sigma^- |1\rangle_k = |0\rangle_k, \sigma^- |0\rangle_k = 0$$

Thus, the hamiltonian for electron - phonon interaction is given by:

$$H_{PE} = -\frac{V_0}{2L^3} \sum_{kk'} (\sigma_{k'}^+ \sigma_k^- + \sigma_k^+ \sigma_{k'}^-) \quad (8)$$

$$\text{or } H_{PE} = -\frac{V_0}{L^3} \sum_k (\sigma_k^+ \sigma_k^-) \quad (9)$$

Thus, the potential is restricted between $\pm \hbar\omega_d$ about the fermi energy. The BCS general eigen state is given by:

$$|\psi_{BCS}\rangle = \prod_k |\psi_k\rangle$$

The potential energy change is given by:

$$\langle \psi_{BCS} | H_{PE} | \psi_{BCS} \rangle = -\frac{V_0}{L^3} \sum_{kk'} v_k u_{k'} u_k v_{k'} \quad (10)$$

Thus, the potential energy decreases due to coupling. On the other hand, the kinetic energy increases by:

$$\langle \psi_{BCS} | H_{KE} | \psi_{BCS} \rangle = \sum_k v_k^2 \epsilon_k \quad (11)$$

where $\epsilon_k = \frac{\hbar^2 k^2}{2m} - E_f^0$. Lets define $W_{BCS} = \sum_k v_k^2 \epsilon_k - \frac{V_0}{L^3} \sum_{kk'} v_k u_{k'} u_k v_{k'}$. The system with minimal W_{BCS} is favourable since a system tries to minimize the total energy. We already know $v_k^2 + u_k^2 = 1$. Thus, minimizing W_{BCS} with respect to v_k , we get:

$$W_{BCS}^0 = \sum_k \epsilon_k \left(1 - \frac{\epsilon_k}{E_k}\right) - \frac{L^3}{V^0} \Delta^2$$

where $\epsilon_k = \frac{\hbar^2 k^2}{2m} - E_f^0$, $\delta = \frac{V_0}{L^3} \sum_{k'} \sin\theta_{k'} \cos\theta_{k'}$, $E_k = \sqrt{\epsilon_k^2 + \Delta^2}$, $v_k = \cos\theta_k$, and $u_k = \sin\theta_k$. The necessary condition for minima is given by :

$$\sin(2\theta_k) = \frac{\Delta}{E_k}$$

Using this, the energy gap can be simplified to give:

$$\Delta E = -\frac{N(E_f^0)\Delta^2}{2} \quad (12)$$

The number of electrons in the system are $n = \frac{N(E_f^0)\Delta}{2}$. Thus, the binding energy of each electron is given by $-\Delta$. Thus, we can say that all the electrons in the system form cooper pairs, and have a net energy gap of Δ for each pair. For weak coupling limit ($N(E_f^0) \ll 1$), Δ can be simplified to give:

$$\Delta \sim 2\hbar\omega_d \exp\left(\frac{-2}{N(E_f^0)V}\right)$$

as shown in eq (6). Condensed matter physics' fundamental Bardeen-Cooper-Schrieffer (BCS) theory accurately describes conventional superconductivity. But it has some serious drawbacks. High-temperature superconductors and materials with complicated underlying mechanisms are not explained by BCS theory, which is mostly applicable to low-temperature superconductors with weak electron-phonon interactions. It simplifies by ignoring effects of magnetic fields, electron-electron repulsion, and non-equilibrium processes. Furthermore, it falls short of explaining the atypical pairing with non-zero angular momentum and the high-temperature superconductivity isotope effect. Despite these flaws, other theories are being researched in order to account for a wider variety of superconducting materials and phenomena. BCS theory is nevertheless crucial for understanding conventional superconductors.

1.2 Ginzberg - Landau Theory

Lets define a order parameter, which is a measure of the degree of order across the boundaries in a phase transition system. This is zero outside the phase transition boundary while non zero within the limits of phase transition boundary.

$$\text{Order parameter} \begin{cases} = 0 & \text{if } T > T_c \\ \neq 0 & T < T_c \end{cases} \quad (13)$$

Let N_s be the concentration of charge carriers in the superconducting state $|\psi(\vec{r})\rangle$. We know the following:

$$N_s \propto \langle \psi(\vec{r}) | \psi(\vec{r}) \rangle \sim |\psi(r)|^2 \quad (14)$$

Expanding the free energy in terms of order parameter:

$$f_s = f_n + \alpha(\psi^2) + \frac{\beta^2 \psi^4}{2} + \dots - \int (\vec{M} \cdot d\vec{B}) + \frac{(-i\hbar\nabla - qA)^2}{2m} \quad (15)$$

where, α, β are constants that needs to be found out and $\psi = \psi(\vec{r})$. For $\vec{B} \rightarrow 0$, and keeping till biquadratic terms, we have:

$$f_n - f_s = \alpha\psi^2 + \frac{\beta\psi^4}{2} \quad (16)$$

Minimizing the free energy with respect to the order parameter (ψ or ψ^*), we get the following relations:

$$(f_s - f_n)_{min} = \frac{|\alpha|^2}{2\beta}$$

$$|\psi|^2 = \frac{|\alpha|}{\beta}$$

Since the critical thermodynamic field is given by:

$$(f_s - f_n)_{min} = \frac{B_c^2}{2\mu_0} \quad (17)$$

Comparing eq 17 with $(f_s - f_n)_{min}$, derived earlier, we get:

$$B_c = \sqrt{\frac{\mu_0 \alpha^2}{\beta}} \quad (18)$$

1.2.1 London penetration depth

The magnetic field is a function of time when it is applied to a superconductor that is initially in zero field. The Maxwell equation states that the time-varying magnetic field generates the electric field. In a regular metal, this will cause eddy currents to form, but in a superconductor, the field will result in supercurrents, which are persistent currents. The magnetic field produced by the induced supercurrents will compete with the applied magnetic field. The flux is completely blocked off from the majority of the superconductor if the applied magnetic field is weak. Perfect diamagnetism is a common term used to describe this phenomena. In superconductors, the London penetration depth (usually denoted as λ or λ_L) characterizes the distance to which a magnetic field penetrates into a superconductor and becomes equal to e^{-1} times that of the magnetic field at the surface of the superconductor.

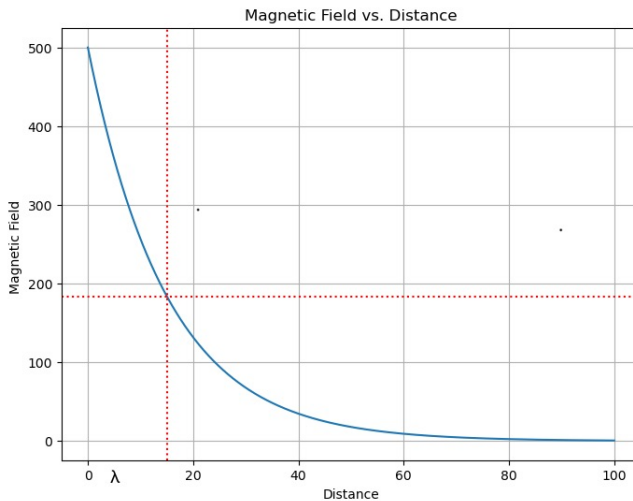


Figure 3. London penetration depth.

The force equation is given by:

$$\mathbf{F} = m \frac{d\mathbf{v}_s}{dt} = -e\mathbf{E} \quad (19)$$

where \mathbf{v}_s is the velocity of the superconducting carrier. The field-induced supercurrent density is given by

$$\mathbf{J}_s = -en_s \mathbf{v}_s, \quad (20)$$

where n_s is the local density of superconducting carriers. Substituting Eq. (20) into Eq. (19) gives

$$\frac{d\mathbf{J}_s}{dt} = \frac{n_s e^2}{m} \mathbf{E} \quad (21)$$

which is known as the "first London equation". Taking the curl of both sides of Eq. (21) gives

$$\frac{m}{n_s e^2} \left(\nabla \times \frac{d\mathbf{J}_s}{dt} \right) = \nabla \times \mathbf{E} \quad (22)$$

which can be rewritten using the Maxwell equation $\nabla \times \mathbf{E} = \frac{-1}{c} d\mathbf{B}/dt$ to give

$$\frac{mc}{n_s e^2} \left(\nabla \times \frac{d\mathbf{J}_s}{dt} \right) + \frac{d\mathbf{B}}{dt} = 0 \quad (23)$$

In order to obtain the Meissner effect (i.e. $\mathbf{B} = 0$ in the bulk of the superconductor) the London brothers removed the time derivative in Eq. (23) and postulated the new equation:

$$\frac{mc}{n_s e^2} (\nabla \times \mathbf{J}_s) + \mathbf{B} = 0 \quad (24)$$

Equation (24) is commonly referred to as the "second London equation". Since the supercurrent density is related to the field \mathbf{B} by another Maxwell equation

$$\mathbf{J}_s = \frac{c}{4\pi} (\nabla \times \mathbf{B}) \quad (25)$$

Substitution of Eq. (25) into Eq. (24) gives

$$\lambda_L^2 (\nabla \times \nabla \times \mathbf{B}) + \mathbf{B} = 0 \quad (26)$$

where

$$\frac{1}{\lambda_L^2} = \frac{4\pi n_s e^2}{mc^2} \quad (27)$$

The variable λ_L is called the London penetration depth, as shown in fig 3. The λ_L^{-2} is proportional to the superfluid density n_s . of Eq. (26) is

$$\mathbf{B}(x) = \mathbf{B}(0) \exp(-x/\lambda_L) \quad (28)$$

Thus, both the magnetic field $B(x)$ and the supercurrent density $J_s(x)$ decay exponentially with distance inside the superconductor over the length scale λ_L .

Thus from λ_L from eq (27), we get:

$$\lambda_L = \sqrt{\frac{m}{\mu_0 q^2 |\psi|^2}} = \sqrt{\frac{m\beta}{\mu_0 q^2 \alpha}} \quad (29)$$

1.2.2 Spatial Variation of order parameter

For a 1-D system with $\vec{B} \rightarrow 0$, we can have:

$$\frac{-\hbar^2}{2m} \frac{\partial^2 \psi}{\partial x^2} + \alpha \psi + \frac{\beta \psi^3}{2} = 0 \quad (30)$$

Minimizing eq(30) and taking $\psi = \psi_\infty f$, where ψ is the state deep inside the superconductor and f is the order parameter. For a system with $f = 1 + g$, where $g \ll 1$ (denotes the strength of the order), we have:

$$f = 1 + g \sim \frac{\psi}{\psi_\infty}$$

and the equation 30 reduces to:

$$\frac{\partial^2 g}{\partial x^2} - 2g \frac{2m\alpha}{\hbar^2} = 0 \quad (31)$$

The factor $\epsilon_{gl} = \sqrt{\left(\frac{\hbar^2}{2m\alpha}\right)}$ is called Gilsberg - Landau coherence length and $g \sim \exp\left(\frac{-x\sqrt{2}}{\epsilon_{gl}}\right)$. Thus, the order develops with the length. Hence, the order increases from 0 at the surface to ψ_∞ deep within the superconductor over the length scale defined by ϵ_{gl} .

There are two competitive processes in the play, a higher London penetration depth increases the overall free energy of the system, while a higher coherence length leads to lowering of the overall free energy. Thus, one can classify TYPE 1 and TYPE 2 semiconductors based on the different length parameters. The G.L parameter is given by:

$$\kappa = \frac{\lambda_L}{\epsilon_{gl}} \quad (32)$$

Thus, we have the following criteria to determine the type of superconductor:

$$\text{Superconductor : } \begin{cases} = \text{TYPE1} & \text{if } \kappa < \frac{1}{\sqrt{2}} \\ = \text{TYPE2} & \text{if } \kappa > \frac{1}{\sqrt{2}} \end{cases} \quad (33)$$

1.3 Josephson junctions and SQUID

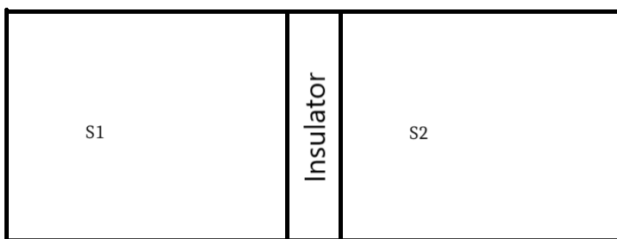


Figure 4. Josephson junction.

Josephson's junction, as shown in 4, is a device that consists of two superconductors weakly coupled by a region which may be either nonsuperconducting or a weaker superconductor. In such devices, a coherent tunneling of cooper

pairs occur, leading to a overall superconductor current, irrespective of the voltage between the two junctions. It is based on the quantum mechanical model of the superconducting state of the metal. The superconducting state $\langle \psi |$ is given by:

$$|\psi\rangle \sim \sqrt{\rho} \exp(i\theta) \quad (34)$$

where ρ is the charge density and θ is the quantum mechanical phase. The josephson junction is the quantum analog of young's double slit experiment. Similar to intensity of the young's double slit experiment being a function of phase difference θ , the josephson current is a function of phase difference between the two quantum mechanical superconducting states, which is eventually a function of magnetic flux ϕ . A remarkable use of josephson junctions is found in superconducting quantum interference device (SQUID) which is a device that measures very low fluctuations in the magnetic field, and works on the principle of josephson junctions. The equations are given by:

$$\frac{-i\hbar\partial\phi_1}{\partial t} = H_1\phi_1 + T\phi_2 \quad (35)$$

$$\frac{-i\hbar\partial\phi_2}{\partial t} = H_2\phi_2 + T\phi_1 \quad (36)$$

Now, suppose, there is a voltage across the insulating region, thus we get:

$$i\hbar n_1 \sin\phi_1 - (\hbar\dot{\phi}_1 + \frac{qu}{2})n_1 \cos(\phi_1) = T\sqrt{n_1 n_2} \cos\phi_2$$

$$i\hbar n_2 \sin\phi_2 - (\hbar\dot{\phi}_2 + \frac{qu}{2})n_2 \cos(\phi_2) = T\sqrt{n_1 n_2} \sin\phi_1$$

Using these, we arrive at the equations:

$$\dot{n}_1 = \frac{2T}{\hbar} \sqrt{n_1 n_2} \sin(\phi_2 - \phi_1) \quad (37)$$

$$\dot{n}_2 = -\frac{2T}{\hbar} \sqrt{n_1 n_2} \sin(\phi_2 - \phi_1) \quad (38)$$

$$\dot{\phi}_1 = -\frac{iT}{\hbar} \sqrt{\frac{n_2}{n_1}} \cos(\phi_2 - \phi_1) - \frac{qu}{2\hbar} \quad (39)$$

$$\dot{\phi}_2 = -\frac{iT}{\hbar} \sqrt{\frac{n_1}{n_2}} \cos(\phi_2 - \phi_1) - \frac{qu}{2\hbar} \quad (40)$$

If the superconductors S1 and S2 are identical, then we get the following:

$$\dot{n}_1 = -\dot{n}_2 = \frac{2T}{\hbar} n \sin(\phi_2 - \phi_1) \quad (41)$$

$$\hbar(\phi_2 - \phi_1) = qu \quad (42)$$

Hence, even in the absence of the voltage, we see a voltage across the josephson junction. The quantum mechanical phase is given by:

$$\phi_2 - \phi_1 = \frac{qu}{\hbar} + \Delta\phi \quad (43)$$

The current across the junction is given by:

$$I_J = \frac{2T}{\hbar} \sin(\omega_j t + \Delta\phi) \quad (44)$$

where, $\omega_j = \frac{2eu}{\hbar}$. With some further calculations, it can be found that:

$$I_J = 2I_0 \sin(\delta) \cos\left(\frac{eN\phi_0}{\hbar}\right) \quad (45)$$

where, $\phi_0 = \frac{\pi\hbar}{e}$. Hence, we see the josephson current maxima for integral multiple of flux quanta.

1.4 Shapiro effect

The current density is given by:

$$J(t) = J_0 \sin(\delta(0) - \omega_j t) \quad (46)$$

When the applied potential u is oscillatory ($u = u_0 + u_a \cos(\omega_a t)$), we get the following equation:

$$J(t) = J_0 \sin(\delta(0) - \omega_j t - \frac{2eu_a}{\hbar\omega_a} \sin(\omega_a t)) \quad (47)$$

This can be simplified to a Bessel's function given by:

$$J(t) = J_0 \sum_{-\infty}^{\infty} B_n \frac{2eu_a}{\hbar\omega_a} \sin(\delta(0) - (n\omega_a + \frac{2eu_a}{\hbar})t) \quad (48)$$

The current density has a time independent DC part and a time dependent AC part. The AC part vanishes for $n\omega_a = -\frac{2eu_a}{\hbar}$. Hence, when we see the IV characteristics, we observe step like graphs between current and potential, which are also termed as **Shapiro steps**. The steps are prominent in the microwave frequencies.

1.5 Resistance vs Temperature characteristics

When the $T > T_c$, then the metal does not act as a superconductor and has a finite resistance. But, as the temperature is lowered, due to formation of cooper pairs, the whole system collapses to a single quantum state and leads to decrease in the resistance. Thus, we see a reduction in the resistance for $T < T_c$

1.6 SQUID chip

A SQUID is a magnetometer that has TYPE 2 superconductor thin film. It has multiple coils to account for modulation and external coupling on a long probe, which is covered by a magnetic shield. The chip contains 2 josephson junctions connected to one another across a voltage source. The SQUID offers Meissner effect, thus restricts any change in the magnetic flux. When there is a change in magnetic field, the

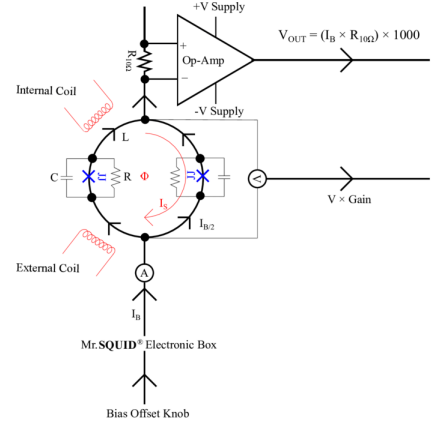


Figure 5. Internal circuit of SQUID chip

SQUID negates the change in flux by applying current in the opposite direction. This current can be measured to find the change in magnetic flux. This further can be used as a DC voltmeter to measure the voltage change in a system. The internal circuitry can be seen in fig 5.

1.6.1 SQUID parameters

Loop inductance parameter: The McCumber parameter measures the trade-off between the SQUID's noise performance and its sensitivity to magnetic flux fluctuations. Although a larger typically denotes a more sensitive SQUID, it can also result in greater noise. This variable aids in the design and optimisation of SQUIDs for certain uses, such as measuring magnetic fields. Mathematically, it is given by:

$$\beta_L = \frac{2\pi L I_c}{\phi_0} \quad (49)$$

Where, L is the inductance of the SQUID loop, I_c is the critical current of the SQUID and ϕ_0 is the magnetic flux quantum. Another way to relate loop inductance parameter is through the equation:

$$\beta_L = \frac{4I_c R_N}{\pi \Delta V} - 1 \quad (50)$$

In order to take into account the fluctuations from temperature, the eq. (50) has some corrections as:

$$\beta_L = \frac{4I_c R_N}{\pi \Delta V} \left(1 - 3.57 \frac{\sqrt{K_b T L}}{\phi_0}\right) - 1 \quad (51)$$

McCumber parameter: A shunt resistance is added to Josephson Junctions to prevent unwanted charging effects, however the capacitance can still ruin the arrangement by causing hysteresis in the current-voltage relation. We can bring a Junction/SQUID closer to perfection if we merely make sure that the shunt resistance is low enough to cancel out the resistive effects. McCumber parameter helps establishes this. Mathematically, it is given by:

$$\beta_c = \frac{2\pi R^2 C}{\phi_0} \quad (52)$$

2. Experimental setup

2.1 Cryogenics

Cryogenics is the science of ultracooling materials from the room temperature. In the experiment, SQUID chip was ultracooled through the use of liquid nitrogen. The liquid nitrogen remains at 77 K, which was poured into a dewar. The SQUID chip was dipped into the dewar to be ultracooled. Use of liquid nitrogen was due to its easy, cheap availability and inert nature.

2.2 SQUID chip

The SQUID chip contains a TYPE 2 superconductor called YBCO ($\text{Y}_1\text{Ba}_2\text{Cu}_3\text{O}_7$). It is placed into a cryogenic probe. The apparatus is wire-bonded to contact pads at the end of the IC chip on which the SQUID chip is mounted in order to conduct transport measurements in the device using the four-probe approach. For electric transport, access is provided to the contact pads. Since SQUID is a very flux-sensitive gadget, it incorporates a conetic alloy produced removable magnetic shield to block any excessive external magnetic flux from entering. Most of the earth's magnetic field is effectively blocked by the mu-metal barrier. An electrical control box with all the circuitry required to run the SQUID is also a part of this system. Its main use is to remove current and magnetic flux from the sample.

2.3 Electrical equipments

Several IC 741, bread board and connecting wires, including BNC cables were used for the observations. Picometer was used as the oscilloscope for measuring the voltage and observing the different characteristics of the signals.

3. Experiment and Observations

3.1 Experiment and problems incurred

3.1.1 IV characteristics

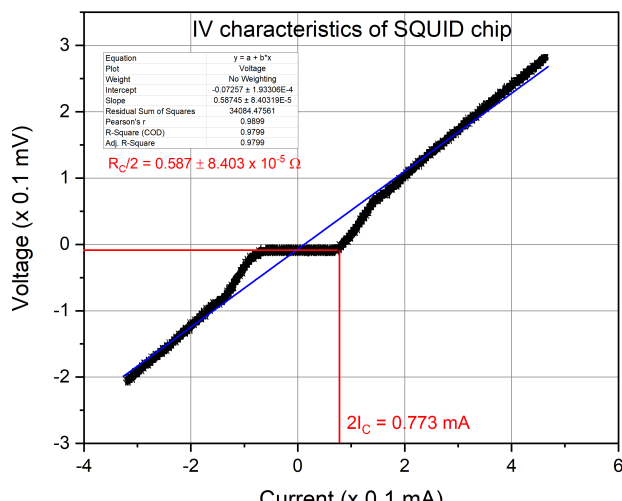


Figure 6. IV characteristics of SQUID chip.

We started the experiment by observing the IV characteristics of the SQUID chip. The YBCO SQUID chip was connected to the electronics box, whose output were connected to picoscope for data visualization. The data was read through the "current" and "voltage" channels of the electronic box. Theoretically, near the zero voltage, there shall be current in the system, due to cooper pair tunneling. The necessary connections were made from the SQUID probe to the electrical box whose output was observed in the picoscope. Experimentally, the results obtained showed that at 0 voltage, there was indeed a current in the system, as shown in fig 6, which was predicted theoretically. No such issues were observed with the setup, although 2 different SQUID chips were used for observation, one of which was later discarded due to erroneous V - ϕ characteristics, thus it took a week to settle down with the experiment.

3.1.2 V - phi characteristics



Figure 7. V - ϕ characteristics of SQUID chip.

Next, the V - ϕ characteristics were studied. The same setup was used, but instead of I - V knob, V - ϕ knob in the electronics box was used to view the characteristics. Initially, on trying to measuring the characteristics, there was too much noise due to which, we could not plot the V - ϕ characteristics. It was mainly due to external noises, from nearby ongoing experiments and other current carrying equipments. To tackle this, the dewar was wrapped with aluminium foil to reduce external noises, as shown in fig 7. The electronic equipments were also kept afar to reduce any external noise. Still, some noise was recorded, as seen in the fig 8. Overall, we still have some noise, due to which the fit is not perfect. Nevertheless, it is enough to support the theoretical prediction of sinusoidal wave patterns.

3.1.3 Shapiro steps

Next, the formation of Shapiro steps were observed. We used wave generator which uses Klystron reflex which uses

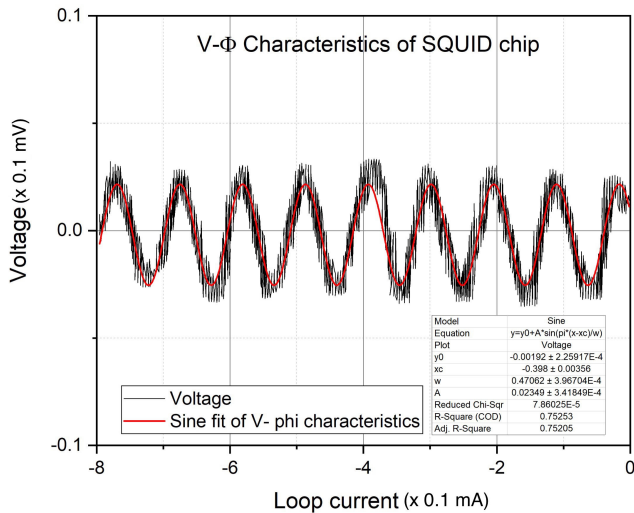


Figure 8. V - ϕ characteristics of SQUID chip.

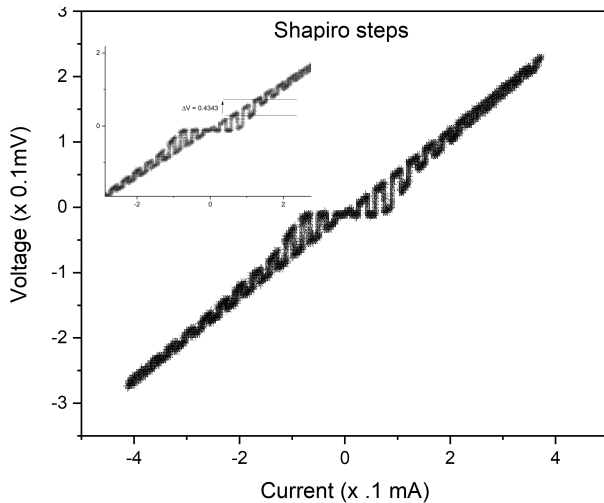


Figure 9. Shapiro steps.



Figure 10. Voltage output through the wavemeter.

oscillation and reflection of electrons at different frequencies to produce microwaves. A frequency meter was used to get the frequency of the wave generator. An oscilloscope was used to measure the change in the output of the frequency meter. We initially got square waveforms, as shown in 10,

which by rotating the frequency meter, reduced to very low voltage due to resonance in the cavity. We found the frequency to be 9.75 ± 0.25 GHz. Next, the frequency meter was set to extreme and the wave produced through wavemeter was used for experiment. This wave was now coupled to the SQUID chip using a BNC cable that was poured into the liquid nitrogen for coupling with the superconductor. The Shapiro steps were observed after some issues with the wave generator. The readings were tough to take since there were some loose connections with the klystron tube, leading to no wave generation. But, after some tries, to push the wire, the generator worked to get the data, as shown in 9. Overall, the steps were observed.

3.1.4 SQUID as a DC voltmeter

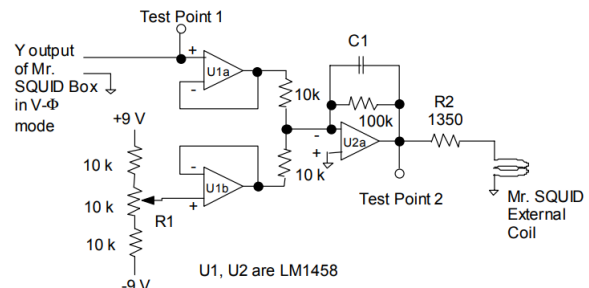


Figure 11. Analog flux locked loop [STAR].

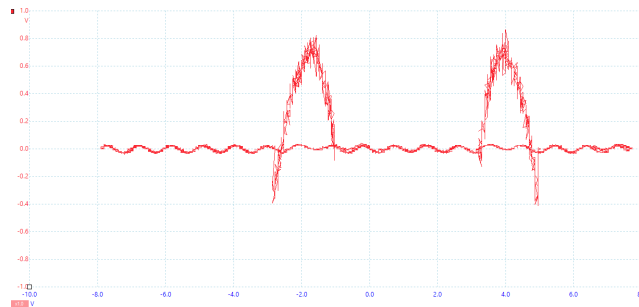


Figure 12. Flux locked loop output.

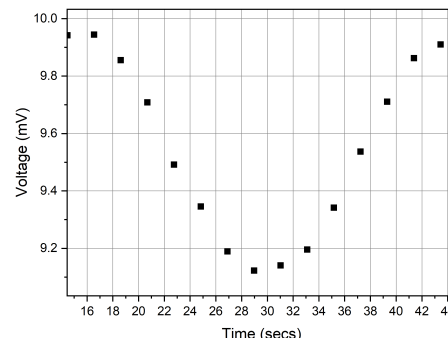


Figure 13. SQUID as DC voltmeter by moving magnet.

In order to convert the SQUID setup into a DC voltmeter, a flux locked loop was necessary. An analog flux locked circuit was designed to understand the basics of the experiment, as shown in fig 11. We faced few issues while designing the circuits as there were issues with connections. The connections had to be redone thrice and rechecked everytime in order to get the desired voltage readings. Finally, it was found that the potentiometer used was a source of most of the noise that made the output irrelevant. Thus, a trimpot potentiometer was used to reduce the noise. Further, the input was changed with two 5 volts batteries (earlier power supplies were being used) in order to reduce further noise. We saw a comparatively better results, which meant the power supply had fluctuations. The corresponding plot is given in fig 12, which has some fluctuations, which were due to potentiometer as when we exchanged it with normal resistors, such fluctuations were absent. We also had to remove some of the in between resistances (10k resistances in fig 11), as they reduced the signals drastically, and the output were flat lines/ noises. We further went on to use the flux locked loop circuit provided by the manufacturer that is has same circuitry made on the breadboard, but with low noise. We planned to use Expise to measure the voltages, to get better readings, but due to time constraints, we used voltmeters to get the overall voltages. We moved a magnet about the SQUID chip, that produced magnetic flux, thus an opposing voltage which was measured using the voltmeter. The fig 13 shows the response of the two josephson junctions to flux change. It was used to get changes of orders of 0.0001 V which is better than normal voltmeters. It can also be utilised to obtain very low fluctuations in the magnetic fields. No specific calculations were made for this part of the experiment, as it was just to understand the working of the SQUID as a DC voltmeter.

3.1.5 Transition temperature of YBCO

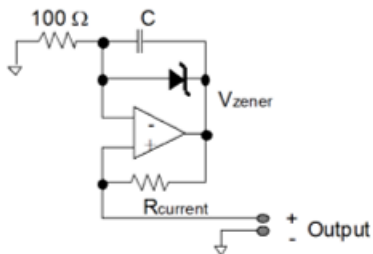


Figure 14. Circuit diagram for a constant current source.

YBCO powder was filled inside a pen cap. It was $\frac{3}{4}$ filled with the powder and black taped to avoid any powder leaks. It was not fully filled, in order to avoid boundary effects. We had to make temperature sensors and a constant current source in order for the temperature sensor to work. Copper wires were chosen as conducting wires due to their low resistivity. Next, a constant current source was made using zener diode and IC 741. The circuit was made according to fig 14. This required some calibrations to get low constant currents, which

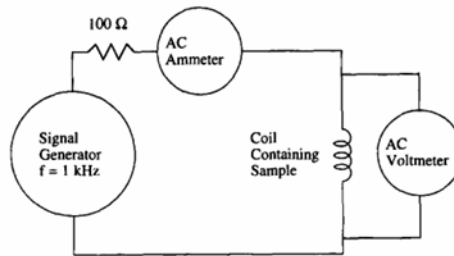


Figure 15. Circuit for measuring resistance through superconductor [Luke].



Figure 16. Setup for YBCO T_c measurement.

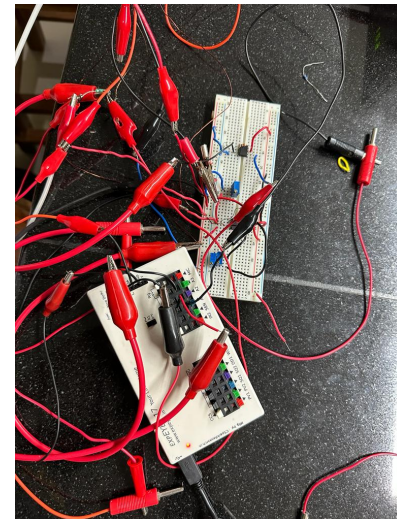


Figure 17. Circuit setup for YBCO T_c measurement using Expise.

was achieved through using potentiometer to vary resistances easily.

Further, a temperature sensor was made to detect the temperature change over time. Since a silicon diode has a linear response to the temperature change, the voltage increases with decrease in temperature, a silicon diode across the constant current source of $10 \mu\text{A}$ was connected. The response of the voltage diode was checked by dipping the diode inside a cryochamber, containing liquid nitrogen. For calibration, the diode, connected with the current source, was dipped in 4 liquids at their freezing temperature which included ethyl alcohol, ice, liquid nitrogen, acetone and the last reading was taken at room temperature. A calibration curve between voltage and temperature was obtained. Now, the system can be manually connected to ammeters and voltmeters to determine the transition temperature. The calibration curve is shown in fig 18.

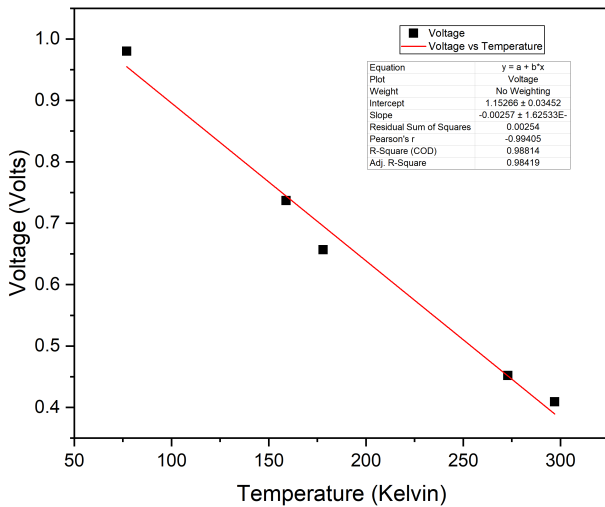


Figure 18. Calibration curve of voltage vs temperature for silicon diode.

As the temperature goes below T_c , the resistance of the superconductor decreases drastically, and also it shows Meissner effect. A coil wound around such a superconductor would experience low induction and thus, the impedance of the circuit decreases. Thus, a stark change in the impedance (ωL) would be noticed when we reach transition temperature. A separate circuit for measuring the current through the coil winding the superconductor was measured referring to fig 15. We faced issues while measuring the current, as the signal was too low, thus an IC 741 was used to increase the amplitude of the signal by 10 fold. This helped to get better current readings. Once the working of both the temperature sensor and superconductor was verified, they were tied together using a black tape and it was assumed that the temperature of the whole system is same, as shown in fig 16. Next, the system was dipped into liquid nitrogen to achieve 77 K temperature and then cooled down at room temperature. The readings were noted as the sample heated back to room temperature.

```

import eyes17.eyes           # uncomment these two lines while running stand-alone
p = eyes17.eyes.open()
import threading
import time

x=[]
y=[]
z=[]
C=1000
def getvalues(x,y,z,C):
    counter = 0
    while C>0.5 or C<0.4:
        print(C)
        if C<0.4:
            if C<0:
                print("Saturated")
                exit
            continue
        time.sleep(0.01)
        A=p.get_voltage('A1')
        B=p.get_voltage('A2')
        C=p.get_voltage('A3')
        x.append(A)
        y.append(B)
        z.append(C)
        counter=counter+2
        if counter%6==0:
            print("working")
    return x,y,z
filename = "data7.txt"
x,y,z = getvalues(x,y,z,C)
with open(filename,'w') as f:
    for i in range(len(x)):
        f.write(f'{x[i]},{y[i]},{z[i]}\n')
print(x,y,z)

```

Figure 19. Python code for acquiring data

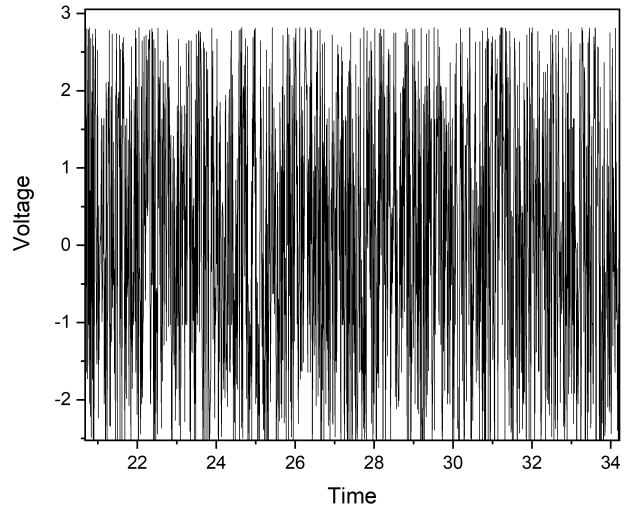


Figure 20. Data for voltage through inductor

We first started with manual readings, but to automate the process, we used Xspice to take all the readings. But, the major issue here was that Xspice measures instantaneous readings and does not give RMS values. A python code was written to get the time stamps along with the values of current across the superconducting circuit and also the temperature sensor and saving in a CSV file. The fig 19 displays the code used to get the values at definite time intervals. Since we expect a sinusoidal graph, we fitted the readings from the superconducting circuit to a sine function to get the RMS value of the system. This RMS value was then taken to find the transition temperature of the YBCO superconductor. The zoomed in observation and fit is given in fig 20 and fig 21 respectively. The data obtained after getting the temperature vs impedance was processed such that random errors in measurement were ig-

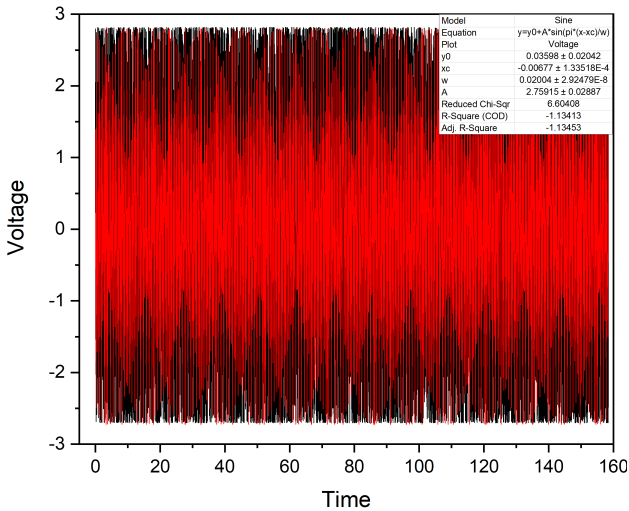


Figure 21. Data fit for voltage through inductor

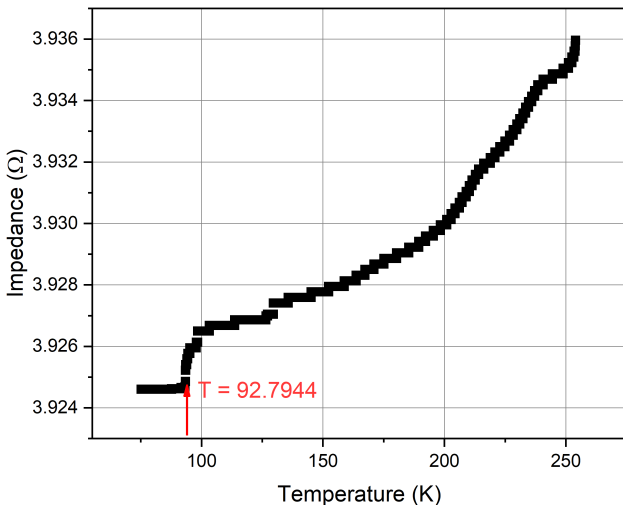


Figure 22. Impedance vs temperature for YBCO

nored through running a python script. Suppose a data point is (251.2546 , 3.934) and the adjacent datapoints are (251.2547, 3.935), (251.2425, 3.935), (251.2558, 3.936). In such case, the point (251.2425,3.935) is incorrect and can be removed since this is an error while measuring the voltage through the instrument. Thus, after data processing, a plot between impedance and temperature was graphed and the kink was noted. Thus, we obtained the final plot as in fig 22, in which, $T_c = 92.7944$ K was determined.

3.2 Analysis and calculations

3.2.1 Critical current, resistance, modulation depth and others

Since two equivalent josephson junction are in play inside a SQUID chip, we get current and resistance contributions from both the junctions. The amplification factor of 10,000 and resistances of 10,000 have been already taken into account to find the I - V characteristics of the SQUID. The slope of

the graph gives the resistances and the knee point gives the corresponding critical current. Thus, we have:

$$R_c = 1.174 \pm 1.6806 * 10^{-4} \Omega, \quad I_c = 38.65 \mu A \quad (53)$$

Modulation depth is the characteristic voltage of the SQUID. This voltage defines the maximum voltage which can be achieved by the SQUID when one quantum of magnetic flux is applied to it. Mathematically, it is given by:

$$V_c = I_c \cdot R_c \quad (54)$$

Hence, using equation(54):

$$\begin{aligned} V_c &= 38.65 * (1.174 \pm 1.6806 * 10^{-4}) mV \\ &= 45.37 \pm 6.495 * 10^{-3} mV \end{aligned}$$

Using equation 49,50 and 51:

$$\beta_L = \frac{2\pi L I_c}{\phi_0} = 8.562$$

$$\Delta \beta_L = \beta_L \frac{\Delta I_c}{I_c} = \frac{0.01}{38.65} (8.562)$$

$$\Delta \beta_L = 0.002$$

$$\beta_L = \frac{4I_c R_N}{\pi \Delta V} - 1 = 11.0091$$

and

$$\beta_L = \frac{4I_c R_N}{\pi \Delta V} \left(1 - 3.57 \frac{\sqrt{K_b T L}}{\phi_0}\right) - 1 = 10.8263$$

The values are off by $\sim 25\% - 30\%$, which shows that the $V - \phi$ characteristics had noises which influenced the overall readings. Probably, we could have removed any air that was above the surface, that could have caused some changes in the readings. Thus, we have the loop inductance parameter, $\beta_L = 8.562 \pm 0.002$.

3.2.2 Flux per quanta and inductance

From fig 8, and the data acquired, we can find that $\Delta I = 20.2987 \mu A$ corresponds to a single flux of quanta. This is an important parameter that would be used to find mutual inductance of the circuit. For the circuit, the mutual inductance is given by:

$$M = \frac{\phi_0}{\Delta I} \quad (55)$$

where $\phi_0 (= 2.07 \times 10^{-15} \text{ Wb})$ is the magnetic flux quantum. Thus, the mutual inductance is:

$$M = \frac{2.07 * 10^{-15}}{20.2987} F = 50.9885 pF \quad (56)$$

$$\frac{\Delta M}{M} = \frac{\Delta(\Delta I)}{\Delta I}$$

$$\Delta M = 0.7419 pF$$

Thus, $M = 50.9885 \pm 0.7419 \text{ pF}$

3.2.3 Shapiro steps

For two steps, we have the following equation to get the $\frac{e}{h}$ value:

$$\frac{e}{h} = \left(\frac{v_{mw}}{\Delta V_0} \right) \quad (57)$$

From fig 9, $\Delta V_0 = 0.4343$ mV. The frequency of the wave generator was found to be 9.75 GHz ± 0.25 GHz e. Using this in equation 57, we get:

$$\frac{e}{h} = 2.2449 * 10^{14} \text{ Hz/Volts}$$

The error can be calculated using error in the frequency measurement. Thus, we have:

$$\Delta\left(\frac{e}{h}\right)/\frac{e}{h} = \frac{\Delta v_{mw}}{v_{mw}}$$

$$\Delta\left(\frac{e}{h}\right) = 0.0575 * 10^{14} \text{ Hz/Volts}$$

Hence, we have: $\frac{e}{h} = 2.2449 \pm 0.0575 \times 10^{14}$ Hz/Volts. This is off by theoretical value of $\frac{e}{h}$ by 7.05%. This is within the permissible limits.

3.2.4 Transition temperature of YBCO

For finding the transition temperature, we used the calibration curve to get the temperature values. The error in the calculation of transition temperature is related to the error in the slope of the temperature calibration along with error in impedance. Through observation, the change in the impedance was found for $T = 92.7944$ K. Thus, $T_c = 92.7944$ K.

$$\begin{aligned} \frac{\Delta T_c}{T_c} &= \sqrt{\left(\frac{\Delta m}{m}\right)^2 + \left(\frac{\Delta I}{I}\right)^2} \\ &= 0.0630 \end{aligned}$$

where I is the impedance and m is the slope of the calibration curve 18 Thus, we get $\Delta T_c = 5.846$ K Thus, the final value of critical temperature is $T_c = 92.7944 \pm 5.846$ K.

4. Results

- $R_c = 1.174 \pm 1.6806 \times 10^{-4} \Omega$.
- $I_c = 38.65 \mu\text{A}$
- $\beta_L = 8.562 \pm 0.002$.
- $M = 50.9885 \pm 0.7419 \text{ pF}$.
- $\frac{e}{h} = 2.2449 \pm 0.0575 \times 10^{14} \text{ Hz/Volts}$.
- $T_c = 92.7944 \pm 5.846 \text{ K}$.

5. conclusion

The YBCO based SQUID chip is useful was used to understand the various concepts of superconductivity. Various experiments based on superconductivity were performed. The experiment helped us to get familiarized with SQUID, superconductivity and usage of instruments to set up experiments. Overall, the basics of these topics were studied and understood thoroughly along with exposure to Xspice.

We learned about the direct manifestation of numerous macroscopic (superconductivity) and microscopic (interference) quantum phenomena through this experiment. SQUID demonstrated the actual appearance of interference of wave-forms, whereas superconductors had provided us with a steady wave function in each electrode. Through an uncalibrated temperature sensor, we looked at the transport characteristics of SQUID and how they relate to superconducting transitions. It was highly challenging to calibrate the system in different temperature ranges due to the system's sensitivity to even the smallest movement caused by the small quantity of electricity. The magnetic response demonstrated why SQUIDs are so magnetically sensitive to the order of 1 fluxon. We were successful in demonstrating the steps in the Shapiro steps experiment as well as how these steps alter with frequency. By doing this, we have established that the GHz frequencies alone were what caused the step-like properties. We found the values of the constants achieved were in the acceptable limits of errors and the overall, the experiment was concluded successfully.

6. References

[Luke] Lukefahr, H. G., Priest, V., St. Jean, K. B., Worley, J. S. R., Yeager, C. S., Gajewski, D. A., and Maple, M. B. (1997). A very simple and inexpensive apparatus for detecting superconducting transitions via magnetic screening. In American Journal of Physics (Vol. 65, Issue 2, pp. 132-135). American Association of Physics Teachers (AAPT). <https://doi.org/10.1119/1.18525>.

[Hale] Haleeda, Nur and Awang Kechik, M. and Abd-Shukor, R.. (2016). PJSRR (2016) 2(1): Effect of Yb₂O₃ Nanoparticle Addition on Superconducting Properties of BSCCO (2223)/Ag Tapes by Acetate Precipitation Method. Pertanika Journal of Science and Technology.

[Soha] Sohail, Emaan and Shiraz Ahmad, Muhammad and Anwar, Sabieh. (2019). Experimental Analysis of Superconductivity and Quantum Interference.

[STAR] Mr.SQUID Operational manual by STAR cryoelectronics.

[Kita] Kita, Takafumi. (2015). BCS Theory. 10.1007/978-4-431-55405-99.

[Kite] Kittel, C. (1996) Introduction to Solid State Physics. 7th Edition, John and Wiley, New York, 117-126.

[Cryo] Cyrot, M. (1973). Ginzburg-Landau theory for superconductors. In Reports on Progress in Physics (Vol. 36, Issue 2, pp. 103-158). IOP Publishing. <https://doi.org/10.1088/0034-4885/36/2/001>

7. Appendix

7.1 Klystron wave generator

The klystron's anode is a resonant cavity with perforated grids that allow accelerated electrons to pass through and continue travelling. However, a positive electrode does not go on to capture those electrons. Instead, they are forced to fall back into the cavity grids by a negatively polarised "reflector" as a result. The tube's operating goal is to have these electrons return to the cavity grids at precisely the right moment to strengthen the electric oscillatory field that is already present across these grids. Oscillations in the cavity are stimulated and sustained when this circumstance exists. If coaxial cable is utilised, microwave power is coupled out of the cavity by way of a loop; if a waveguide is used to transmit the power to the load, microwave power is simply coupled out of the cavity through an appropriate aperture. The spent electrons fall back to the positively biassed control grid where they are collected, adding to the control grid current after the electrons' kinetic energy has been given up to the oscillatory field of the cavity. When the tube is not oscillating, a significant amount of electrons are deflected by the reflector's retarding field with enough energy to travel through the cavity grids and subsequently be captured by the control grid. The oscillating electric field that appears across the cavity grids, nevertheless, absorbs most of the energy from falling electrons when oscillations are sustained in the cavity. Such electrons are then captured by the cavity grids, which serve as the equivalent of the diode's plate in this context.

7.2 Frequency meter

The principle of electromagnetic wave resonance inside a closed cavity governs the operation of a frequency metre cavity, also referred to as a microwave resonator. It is frequently employed for accurate radio frequency and microwave measurements. The cavity is filled with a sample of the signal that has to be measured, as shown in fig 23. By altering its dimensions, the cavity is brought into resonance at a particular frequency. The electromagnetic field inside the cavity is enhanced when the signal's frequency coincides with the cavity's resonant frequency, which results in a drop in output power. The position of the dip can be measured to identify the resonant frequency, which enables precise frequency monitoring of the input signal.

7.3 Seelab

Several physical parameters, including as voltage, current, frequency, resistance, capacitance, and inductance, can be



Figure 23. Setup of frequency meter

measured using SEELab 3.0. Additionally, it may be used to create waveforms, manage other devices like motors, and communicate with I2C and SPI modules. It comprises of a main board with a built-in breadboard slot and a 40-pin connector. This makes it simple for users to connect and test out a range of sensors and modules. It can be used to perform a wide range of experiments, from simple circuit measurements to complex data analysis. SEELab 3.0 is also a great tool for troubleshooting and development. It can be used to debug circuits, test components, and prototype new designs.